Background activity drives criticality of neuronal avalanches

2007 J. Phys. A: Math. Theor. 40 9297

(http://iopscience.iop.org/1751-8121/40/31/008)

IOP PUBLISHING JOURNAL OF PHYSICS A: MATHEMATICAL AND THEORETICAL

J. Phys. A: Math. Theor. **40** (2007) 9297–9309 doi:10.1088/1751-8113/40/31/008

Background activity drives criticality of neuronal avalanches

D E Juanico and C Monterola

National Institute of Physics, University of the Philippines, Diliman, Quezon City 1101, Philippines

E-mail: djuanico@gmail.com

Received 12 February 2007, in final form 18 June 2007
Published 19 July 2007
Online at stacks.iop.org/JPhysA/40/9297

Abstract

We establish a general framework that explains how leaky, dissipative systems, such as neuronal networks (NN), can exhibit robust self-organized criticality (SOC). Consistent with recent experiments, we propose that persistent membrane potential fluctuations allow NNs to transform from a sub-critical to a critical state. Our results also account for the tendency in small networks to tip towards an epileptiform state (the case of largely synchronized neurons) when background activity is strong.

PACS numbers: 05.65.+b, 87.19.La, 89.75.Da

(Some figures in this article are in colour only in the electronic version)

1. Introduction

Recent, concrete, experimental evidence for SOC in real systems has been found by studies of rat brain tissue slices. A new type of spontaneous (i.e., self-organized) activity, dubbed as *the neuronal avalanche*, has been observed by using a micro-electrode array superficially placed over the brain tissue surface [1]. Measurements of neuronal avalanche size reveal a decreasing power-law size distribution with exponent $\approx -3/2$. The neuronal avalanche has been proposed as an optimal mode for high-speed information transmission and as a possible substrate for memory [1–3].

The problem in binding this remarkable experimental phenomenon to the current SOC framework is the fact that information propagation between neurons (analogous to sandpile grain transfer) is highly non-conservative [4, 5]. This finding contends with the longstanding SOC hypothesis that asserts the irreconcilability between criticality and non-conservation. Common among paradigmatic SOC models is their incapability of simultaneously satisfying conditions for both criticality and non-conservation.

Tsuchiya and Katori offered a rigorous proof that violation of the grain-transfer conservation law foils the criticality of Abelian sandpile models [6]. An elegant mean-field treatment of the Manna model known as the self-organized branching process (SOBP)

introduced by Zapperi, Lauritsen and Stanley further asserts that criticality is disrupted by any level of non-conservation apart from boundary dissipation [7, 8]. Breaking of SOC due to non-conservation has also been demonstrated analytically and numerically in the Olami–Feder–Christensen earthquake model [9]. The forest-fire model (FFM) proposed by Drossel and Schwabl is not constrained by any conservation law, and might have been a promising non-conservative SOC model. Ultimately, it was proven, by means of Lyapunov exponent analysis [10] and later via renormalization group methods [11], that FFM is not self-organized and thus its critical behaviour is not SOC. Therefore, any attempt to subsume critical phenomena in a variety of real self-organizing physical systems that evidently violate conservation laws, such as neuronal networks, needs to circumvent the conceptual barricade that forbids any non-conservative system from achieving SOC. Attempts in this direction had been inconclusive, by relying heavily on numerical evidence [12] or ascribing non-conservation to a non-transferred variable [13]. Recently, Juanico *et al* [14] demonstrated the possibility of attaining SOC in sandpile systems despite violation of conservation law during avalanches.

The present work thoroughly applies Juanico *et al* mean-field analysis [14] in the context of neuronal systems. We consider a neuronal network driven by background activity or membrane potential fluctuations as a contributory SOC mechanism in neuronal systems. The role of membrane potential fluctuations treated as noise has been previously proposed as the salient mechanism that allows efficient functioning of neural networks [15]. While our previous work [14] analysed the density of active (threshold-state) components, in this paper we look into the branching ratio, which is the parameter more relevant to the experiments conducted by Beggs and Plenz [1]. We also demonstrate the occurrence of epileptiform activity (or supra-critical behaviour) as a result of intensified neuronal membrane-potential fluctuations. The findings presented here provide useful insight into how non-conservative, leaky, dissipative systems such as neuronal networks can possibly maintain a critical state in accord with SOC principles.

2. NNnM: noisy neuronal network model

2.1. Sandpile formalism of neuronal phenomena

An individual neuron is modelled as a binary 'ON-OFF' switch and its state $|\psi\rangle$ is defined by mapping $\{|\psi\rangle\} = \{|0\rangle, |1\rangle, |2\rangle\}$ to its membrane potential V_{mem} with reference to the *resting potential* V_{rest} and the *threshold potential* V_{thresh} in the following:

- Dormant state: $|0\rangle \mapsto V_{\text{rest}} \leqslant V_{\text{mem}} < V_{\text{thresh}}$
- Threshold state: $|1\rangle \mapsto V_{\text{mem}} = V_{\text{thresh}}$
- Excited state: $|2\rangle \mapsto V_{\text{mem}} > V_{\text{thresh}}$.

The above mapping concords with Manna's sandpile model [16]. Hereby, $|2\rangle$ is a transient ON state, whereas $|0\rangle$ and $|1\rangle$ are OFF states.

The neurophysiological distinction between the dormant and threshold states lies in voltage-dependent neuronal-membrane permeability to two different ions, namely Na^+ and K^+. At rest, the permeability of the neuronal plasma membrane is much higher for K^+ than for Na^+, implying a net efflux of K^+ across the membrane. In the dormant state, as the membrane potential is increased, the permeability for Na^+ passively increases, causing an increase of Na^+ influx relative to K^+ efflux. The point at which Na^+ inflow just equals K^+ outflow represents an unstable electrochemical equilibrium. The behaviour of the membrane of a neuron at the threshold state reflects this instability. In addition, the membrane potential may linger at the threshold level for a variable amount of time before either returning to the resting level or

erupting into an action potential [17]. In theory, if there is a net internal gain of a single Na^+ ion, the threshold neuron becomes excited; conversely, the net loss of a single K^+ ion brings the threshold neuron back to the dormant state.

At the threshold state, the current carried by Na^+ entering the neuron is exactly equal to the K^+ current that is flowing out. Once the threshold neuron is excited, the increase in Na^+ influx becomes self-sustaining and an action potential is fired. However, the action potential is a brief event because Na^+ channels on the membrane do not remain open for very long, and voltage-dependent K^+ channels open at about the same time as the Na^+ channels close, so that K^+ now flows out the neuron again, and the neuron consequently de-excites. The excited state is therefore highly unstable [17, 18].

Grain creation and annihilation operators of the Abelian sandpile are associated with neuronal processes known as *depolarization* and *hyperpolarization*, respectively. Depolarization displaces V_{mem} towards a lower (more negative) value, whereas hyperpolarization raises V_{mem} towards a higher (less negative) value [17, 18]. In sandpile terms, both processes are formulated as $\mathcal{G}^\dagger|\psi\rangle = |\psi+1\rangle$ for depolarization and $\mathcal{G}|\psi\rangle = |\psi-1\rangle$ for hyperpolarization.

2.2. Neuronal avalanche rules

The system is a noisy neuronal network assumed to be fully-connected and non-recurrent, i.e., each neuron links to every other neuron but not to itself. Although fully connected, a maximum of only two randomly chosen synaptic connections per neuron are activated in a single avalanche. The network has size $N = 2^{n+1} - 1$, where n is the upper bound on the number of generations of depolarization in one avalanche sequence. Thus, n may be interpreted as a boundary condition, in accord with the definition of boundaries employed in the SOBP model [7].

The entire network is *quiescent* when no $|2\rangle$-neurons are present; otherwise it is *activated*. Let us define the density of $|0\rangle$ and $|1\rangle$ neurons in a quiescent network as $1-\rho$ and ρ, respectively. The quiescent network is 'slowly stimulated' at time t via rule A, defined as follows:

(1) Choose a neuron w at random.
(2) Depolarize chosen neuron: $\mathcal{G}^\dagger|\psi_w\rangle$.

If $|\psi_w\rangle = |0\rangle$, rule A is repeated in the next time step and another neuron is randomly selected. The probability that A finds a $|1\rangle$-neuron at time t is $\rho = \rho(t)$. When this happens a $|2\rangle$-neuron emerges, and consequently time is frozen and avalanche ensues. Freezing of time follows from the assumption that the ensuant avalanche event takes place instantaneously with respect to the rate at which A is applied—the essence of 'slow stimulation', which is conventionally referred to as *infinite time-scale separation*. This is justified by the fact that the time interval between two distinct avalanche sequences is much longer than the duration of a single avalanche sequence [1]; more will be discussed about this issue in section 5.2. Infinite time-scale separation is also a typical assumption in sandpile models [19].

The ensuant events following the emergence of a $|2\rangle$-neuron are collectively referred to as rule B, defined as follows:

(1) Randomly choose two post-synaptic neurons (u and v) connected to $|2\rangle$-neuron w.
(2) After firing an action potential, w immediately hyperpolarizes, and u and v may depolarize. Three possible cases:
   (a) With probability α: $\mathcal{G}\mathcal{G}|\psi_w\rangle$, and $\mathcal{G}^\dagger|\psi_u\rangle$ and $\mathcal{G}^\dagger|\psi_v\rangle$.
   (b) With probability β: $\mathcal{G}|\psi_w\rangle$, and either $\mathcal{G}^\dagger|\psi_u\rangle$ or $\mathcal{G}^\dagger|\psi_v\rangle$.

(c) With probability $\epsilon = 1 - \alpha - \beta$: $\mathcal{G}\mathcal{G}|\psi_w\rangle$, but neither u nor v depolarize.

(3) Repeat B.1 and B.2 until all $|2\rangle$-neurons depleted, or after n generations of depolarization are reached.

(4) Resume rule A.

Rule B essentially describes the avalanche sequence, which only terminates if the activated network relaxes back to its quiescent state (i.e., no $|2\rangle$-neurons present), or after the boundary condition (i.e., n generations of depolarization) is met. Time takes off again after B terminates and once more the network builds up for the next avalanche event via rule A. The total number s of neurons depolarized during the sequence is defined as *avalanche size*.

2.3. Background activity

The presence of background activity is the distinguishing characteristic of NNnM—the system is a *noisy* neuronal network. Background activity or membrane potential fluctuations present in the quiescent network is motivated by electrophysiological studies of a *hyperpolarization-activated cation current*, or simply H-current [20]. Kang, Kitano and Fukai have demonstrated, using a realistic model of a cortical network [20], that sub-threshold membrane potential fluctuations 'can be generated through a spike-timing-dependent self-organizing process in a network of inhibitory neurons and excitatory neurons expressing the H-current.' Spike-timing-dependent processes that affect the probability with which a neuron fires an action potential have also been investigated experimentally by whole-cell recordings of cortico-striatal slices [21]. The existence of membrane potential fluctuations is also linked to the presence of background noise in neuronal activity, which has been found to play a significant role to the enhanced neuronal responsiveness to varying stimuli intensity (see [22] for a review). Background noise acts analogously to the noise in *stochastic resonance*, a nonlinear phenomenon with an extensive following in the neuroscience and computational neuroscience research community [15, 23].

The level of background activity in the quiescent network is quantified by a parameter $\eta \in (0, 1]$. Background activity is implemented via rule C as follows:

(1) With probability η: $\mathcal{G}^\dagger|0\rangle$.

(2) With probability $\eta(\sigma/\rho - 1)$: $\mathcal{G}|1\rangle$

where σ that appears in C.2 is known as the *branching parameter*, to be discussed in more detail in section 3. At time t, rule C operates in parallel over the entire network and is concurrent with rule A. It changes $\rho(t)$ in the next time step $t + \Delta t$ such that C.1 contributes, on the average, a change

$$\rho(t + \Delta t) - \rho(t) = \eta[1 - \rho(t)]\Delta t, \tag{1}$$

and C.2 contributes

$$\rho(t + \Delta t) - \rho(t) = -\eta\left[\frac{\sigma(\rho(t))}{\rho(t)} - 1\right]\rho(t)\Delta t, \tag{2}$$

where σ/ρ is the local branching parameter. Since C.1 and C.2 happen concurrently, then (1) and (2) can be added together to yield a net change in ρ per unit time

$$\mathcal{B}(\rho; \eta) = \eta[1 - \sigma(\rho)]. \tag{3}$$

Equation (3) is our phenomenological model of background activity, which only has one free parameter η in contrast to two-parameter definition by Juanico *et al* [14]. $\mathcal{B}$ is excitatory (i.e., increases ρ) when $\sigma < 1$, and inhibitory (i.e., decreases ρ) when $\sigma > 1$. Experimental studies found that this seesaw between cortical excitation and inhibition contributes to the stability of neuronal networks, keeping them at the border between inactivity and epileptiform activity [5].

Table 1. NNnM transition rules and corresponding transition probabilities. State $|\psi_u\psi_v\psi_w\rangle$ is just $|\psi_u\rangle$, $|\psi_v\rangle$ and $|\psi_w\rangle$ taken together to describe the neighbourhood of neuron v and its two post-synaptic neurons u and w. The sum of transition probabilities for the avalanche and non-conservation rules is $\rho(t)$, which is the probability that the avalanche had initiated at time t.

Process	Rule	Transition probability, p
Background activity	$\|1\rangle \to \|0\rangle$	$\eta(\sigma/\rho - 1)\rho$
	$\|0\rangle \to \|1\rangle$	$\eta(1-\rho)$
Neuronal avalanche	$\|121\rangle \to \|202\rangle$	$\alpha\rho^3$
	$\|021\rangle \to \|102\rangle$	$2\alpha\rho^2(1-\rho)$
	$\|020\rangle \to \|101\rangle$	$\alpha\rho(1-\rho)^2$
	$\|121\rangle \to \|112\rangle$	$\beta\rho^3$
	$\|021\rangle \to \|012\rangle$	$2\beta\rho^2(1-\rho)$
	$\|020\rangle \to \|011\rangle$	$\beta\rho(1-\rho)^2$
Non-conservation	$\|2\rangle \to \|0\rangle$	$\epsilon\rho = (1-\alpha-\beta)\rho$

3. NNnM dynamics and branching process

The NNnM transition rules B and C are summarized in table 1. Background activity is from C. First three avalanche rules are from B.2.a, whereas the last three are from B.2.b. Non-conservation rule is from B.2.c., so that ϵ measures the level of non-conservation of NNnM. Conservation law is violated when $\epsilon > 0$.

The density ρ, assumed to be a continuous dynamical variable, satisfies

$$\frac{\mathrm{d}\rho}{\mathrm{d}t} = \mathcal{B}(\rho;\eta) + \mathcal{A}(\rho;\epsilon) + \chi(t). \tag{4}$$

The noise term $\chi(t)$ arises from the stochastic nature of NNnM transition rules, and accounts for fluctuations around average values assumed to hold in the mean-field. $\chi(t) \to 0$ in the large-N limit, which we have confirmed through numerical simulations. The term $\mathcal{A}(\rho;\epsilon)$ represents the net change in $\rho(t)$ due to an avalanche at time t. Treating the neuronal avalanche as a branching process, and following closely the analysis in [8], $\mathcal{A}$ satisfies

$$N\mathcal{A} = 1 - \sigma^n - \frac{\epsilon\rho}{1-(1-\epsilon)\rho}\left[1 + \frac{1-\sigma^{n+1}}{1-\sigma} - 2\sigma^n\right], \tag{5}$$

where the first term on the right-hand side is due to rule A acting on a $|1\rangle$-neuron. The second term is the average dissipated stimuli from $|1\rangle$-neurons becoming $|2\rangle$ in the nth generation. The third term, which is only non-zero when $\epsilon > 0$, is the average dissipated stimuli lost due to non-conservation. The branching parameter σ is derived from the definition

$$\sigma = \sum_k kq(k), \tag{6}$$

wherein, from table 1, the branching probability $q(k)$ that a hyperpolarizing $|2\rangle$-neuron consequently depolarizes k other neurons is

$$q(k) = \alpha\rho\delta_{k,2} + \beta\rho\delta_{k,1} + [1-(1-\epsilon)\rho]\,\delta_{k,0}, \tag{7}$$

with $\delta_{i,j}$ being the Kronecker delta. The first and second terms in (7) are the total transition probabilities of the first three avalanche rules and of the last three avalanche rules listed in table 1, respectively. The last term is the sum of the probability for non-conservation and the probability that a $|0\rangle$-neuron has been depolarized, which both yield $k = 0$. Substitution of (7) to (6) renders

$$\sigma = (2\alpha + \beta)\rho, \tag{8}$$

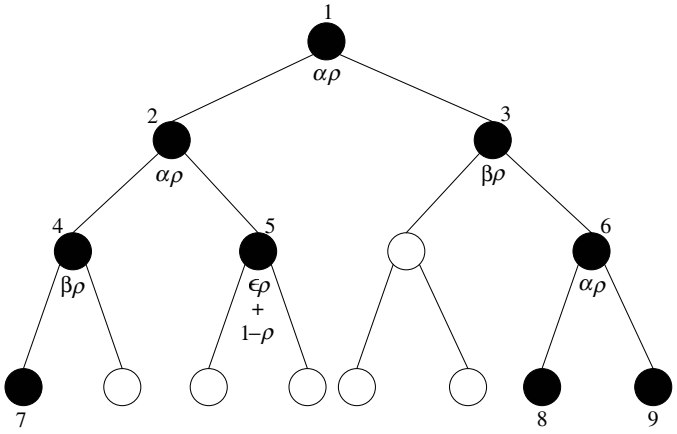

Figure 1. Avalanche represented as a binary branching tree with $n = 3$ (or $N = 2^4 - 1 = 15$). Shaded circles represent depolarized ($\mathcal{G}^\dagger|\psi\rangle$) neurons. All shaded circles are labelled chronologically. Avalanche size $s = 9$ is the total number of shaded circles.

which depends on α and β, and is proportional to density ρ. In this model it is assumed that α and β remain fixed throughout so that the only dynamic variable is ρ. Consequently,

$$\frac{\mathrm{d}\sigma}{\mathrm{d}t} = (2\alpha + \beta)\frac{\mathrm{d}\rho}{\mathrm{d}t}. \tag{9}$$

A branching process is sub-critical when $\sigma < 1$, for which avalanches have sizes no larger than a finite cutoff size irrespective of how large the system is. On the other hand, a branching process is supra-critical when $\sigma > 1$ such that avalanches as large as the system itself are formed with a relatively high probability. Hence, $\sigma = 1$ is a critical value that results to a critical branching process [24], from which a power-law size distribution is expected.

4. Neuronal avalanche size distribution

Figure 1 is a diagram of the branching-tree representation of an avalanche. Node 1 corresponds to the initial $|2\rangle$-neuron emerging from rule A at time t with probability $\rho(t)$. During the avalanche, it depolarizes two $|1\rangle$-neurons (nodes 2 and 3) with probability $\alpha\rho$, both becoming excited. Node 3 subsequently depolarizes one neuron (node 6) with probability $\beta\rho$. Node 5 represents either a hyperpolarizing $|2\rangle$-neuron that is non-conservative with probability $\epsilon\rho$, or an initially $|0\rangle$-neuron before it was depolarized with probability $1 - \rho$ by node 2. Setting $n = 3$, all excited neurons at three levels below the topmost node do not further depolarize other neurons. In the example shown, the avalanche size is $s = 9$.

With $q(k)$ the avalanche size distribution $P(s)$ is calculated using a generating functional formalism. A generating function $\mathcal{F}_m(\omega)$ of $P(s)$ after m generations is defined as

$$\mathcal{F}_m(\omega) = \sum_{s=1}^{\infty} P(s)\omega^s. \tag{10}$$

$\mathcal{F}_m$ also happens to be the mth iterate of the generating function $\mathcal{F}_1 := \mathcal{F}$

$$\mathcal{F}(\omega) = \sum_{s=1}^{\infty} q(s-1)\omega^s = \omega \sum_{s=1}^{\infty} q(s-1)\omega^{s-1}. \tag{11}$$

Furthermore, by definition $\mathcal{F}_{m+1}(\omega) = \mathcal{F}[\mathcal{F}(\omega)]$, such that from (11), the following sufficiently holds [24]

$$\mathcal{F}_{m+1}(\omega) = \omega \sum_{s=1}^{\infty} q(s-1)[\mathcal{F}_m(\omega)]^{s-1}, \tag{12}$$

which simplifies to

$$\mathcal{F}_{m+1}(\omega) = \omega\left\{\alpha\rho\mathcal{F}_m^2 + \beta\rho\mathcal{F}_m + [1-(1-\epsilon)\rho]\right\}, \tag{13}$$

following from (7). For sufficiently large m, the theory of branching processes asserts a self-consistency relation $\mathcal{F}_{m+1} \simeq \mathcal{F}_m$, so that solving for $\mathcal{F}_m$ in (13) yields

$$\mathcal{F}_m(\omega) = \frac{1 - b\omega - \sqrt{1 - 2b\omega + a\omega^2}}{2\alpha\rho\omega}, \tag{14}$$

where $a = \beta^2\rho^2 - 4\alpha\rho[1-(1-\epsilon)\rho]$, and $b = \beta\rho$. Binomial expansion of (14) around its singularity $\omega = 0$ yields a power series of the form defined in (10). The coefficients of expansion correspond to $P(s)$. In a more compact form the solution can be expressed as a recurrence relation

$$P(s) = \frac{1}{s+1}\left[(2s-1)bP(s-1) - (s-2)aP(s-2)\right]. \tag{15}$$

In particular, Pinho and Prado [25] have calculated an analytic form of (15) for the special case of $\beta = 0$. Equation (15) can easily be demonstrated, by suitable application of Stirling's relations, to have the asymptotic behaviour $P(s) \sim s^{-3/2}$ for $s \gg 1$ if $a = 2b - 1$, a condition that can equivalently be expressed as

$$\begin{aligned} Q(\rho) &= a - 2b + 1 \\ &= \beta^2\rho^2 - 4\alpha\rho[1-(1-\epsilon)\rho] - 2\beta\rho + 1 \\ &= 0. \end{aligned} \tag{16}$$

Since $\sigma \propto \rho$ from (8), then (16) can also be expressed as $Q(\sigma)$ with root at $\sigma = 1$, which is the critical value of the branching parameter.

Numerical simulations of the NNnM also confirm the predicted asymptotic behaviour of $P(s)$. Figure 2 shows the probability and cumulative distributions of avalanche sizes for a system of $N = 131\,071$ neurons with degree of non-conservation $\epsilon = 0.2$ and background intensity $\eta = 0.031\,25$. The frequency distribution is a straight line with slope $-3/2$ in double-logarithmic scale for a certain range of avalanche sizes, whereas the cumulative distribution is similarly a straight line with slope $-1/2$. A power-law frequency distribution with exponent τ is expected to yield a cumulative distribution with exponent $\tau + 1$ [26].

5. Results and discussion

The stationary behaviour of NNnM is examined using a well-established geometrical theory of fixed points [27]. Nonlinear differential equations such as (9) may be analysed graphically in terms of vector fields. In this framework, $\dot{\sigma} := \mathrm{d}\sigma/\mathrm{d}t$ is interpreted as a 'velocity vector' at each possible σ value. A plot of $\dot{\sigma}$ versus σ is known as the phase portrait of the model. The fixed point σ^* corresponds to the σ-value at which $\dot{\sigma} = 0$. The trajectory of the vector around the neighbourhood of this fixed point is directed to the right where $\dot{\sigma} > 0$, and to the left where $\dot{\sigma} < 0$. This means that if $\dot{\sigma}$ is increasing around the neighbourhood of σ^*, then the fixed point is repulsive. On the other hand, if $\dot{\sigma}$ is decreasing, then the fixed point is attractive. Linearization of (9) actually yields

$$\lim_{\sigma\to\sigma^*} \frac{\partial}{\partial\sigma}\frac{\mathrm{d}\sigma}{\mathrm{d}t} < 0,$$

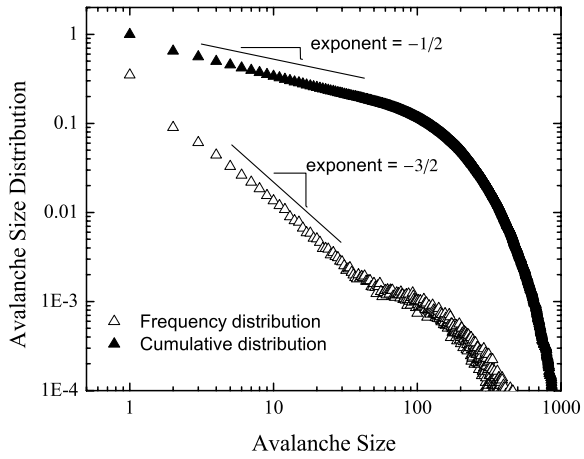

Figure 2. Typical distribution of avalanche sizes for an NNnM system of size $N = 131\,071$ ($\epsilon = 0.2$ and $\eta = 0.031\,25$). The exponents of both frequency (△) and cumulative (▲) distributions conform to power-law behaviour.

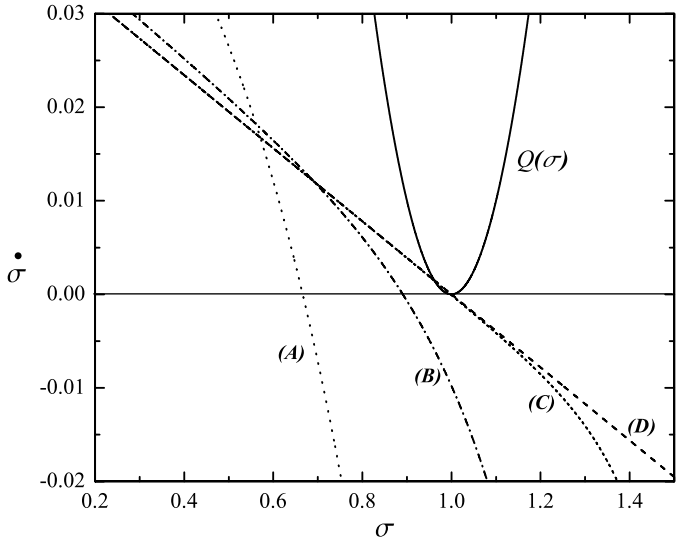

Figure 3. Phase portrait of NNnM, showing $\dot{\sigma}$ versus σ ($\epsilon = 0.25$ and $\eta = 0.031\,25$), for different sizes: (A) $N = 2^5 - 1 = 31$ ($\cdots\cdots$); (B) $N = 2^9 - 1 = 511$ (— · —), (C) $N = 2^{17} - 1 = 131\,071$ (- - - -); (D) $N = 2^{53} - 1 \to \infty$ (– – –). Fixed points σ^* corresponds to the roots of $\dot{\sigma}(\sigma)$. Also shown is $Q(\sigma)$ with root at $\sigma = 1$.

which further implies that the fixed points of (9) are attractive. Shown in figure 3 are the phase portraits derived by numerically solving (9) for $\epsilon = 0.25$ and $\eta = 0.031\,25$, and for different sizes N. All phase portraits are monotonically decreasing. Therefore, the network spontaneously approaches (without the tuning of control parameters) the state defined by its fixed point—the essence of self-organization.

Also illustrated in figure 3 is the parabolic function $Q(\sigma)$ with a root at $\sigma = 1$. For networks with size $N = 31$ and $N = 511$, obviously $\sigma^* < 1$, implying that they self-organize towards sub-critical states. However, for $N = 131\,071$ up to $N \to \infty$, $|1 - \sigma^*| \ll 1$. A large

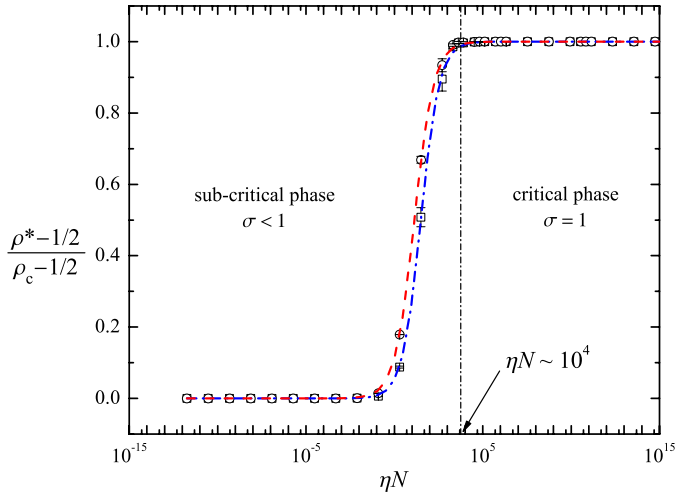

Figure 4. Phase transition in the NNnM. Data points result from numerical analysis of the fixed point ρ^* of (4) neglecting the noise term $\chi(t)$, for: $\epsilon = 0.2$ (□) and $\epsilon = 0.46$ (○), and various $\eta \in (0, 1]$ and system size N. The critical density $\rho_c = (2\alpha+\beta)^{-1}$ is derived from (8) with $\sigma = 1$. The curves are logistic fits of the form $y(x) = 1-[1+(x/\theta)^\gamma]^{-1}$, where $y = (\rho^*-1/2)/(\rho_c-1/2)$ and $x = \eta N$.

non-conservative network achieves SOC even if its size is finite. The rapid approach of σ^* towards 1 from $N = 511$ to $N = 131\,071$ in addition to the decelerating change in σ^* from $N = 131\,071$ to $N \to \infty$ are indicative of a phase transition.

5.1. Phase transition

Indeed, as shown in figure 4, NNnM exhibits a phase transition. The data points are derived from numerical fixed-point analysis of (4) for $\epsilon = 0.2$ and $\epsilon = 0.46$, assuming that the noise term $\chi(t)$ is too small to be significant. For a wide range of background activity $\eta \in (0, 1]$, a phase diagram emerges from the relation between $(\rho^* - 1/2)/(\rho_c - 1/2)$ and ηN. The resultant plots are fitted by a logistic curve

$$\frac{\rho^* - 1/2}{\rho_c - 1/2} = 1 - \left[1 + \left(\frac{\eta N}{\theta}\right)^\gamma\right]^{-1}, \tag{17}$$

wherein ρ^* is the steady-state density corresponding to the fixed-point branching parameter σ^*, and ρ_c is the critical density derived from (8) with $\sigma = 1$. The fitting parameters are $\theta = 31.36 \pm 0.65$ and $\gamma = 0.84 \pm 0.01$ (goodness of fit: $\chi^2/\mathrm{DoF} = 2 \times 10^{-5}$, $R^2 = 0.9999$, no weighting) for $\epsilon = 0.2$, and $\theta = 13.49 \pm 0.23$ and $\gamma = 0.80 \pm 0.01$ (goodness of fit: $\chi^2/\mathrm{DoF} = 1 \times 10^{-5}$, $R^2 = 0.999\,94$, no weighting) for $\epsilon = 0.46$. Both fits are closely similar albeit the ϵ-values are quite disparate. This implies that the phase transition of the NNnM is minimally sensitive to variations in the level of non-conservation ϵ.

Equation (17) suitably describes two limiting cases of the model. The first one is $\eta \to 0$, which results to $\rho^* \to 1/2$. This limiting case is equivalent to having no background activity, as in the SOBP model by Lauritsen, Zapperi and Stanley [8]. They have similarly found that the steady-state density $\rho^* = 1/2$, irrespective of any level of non-conservation ϵ. Consequently, the SOBP model is always sub-critical (i.e., yields no power-law but rather exponentially truncated distributions) whenever $\epsilon > 0$. Therefore, a neuronal network without background activity cannot display SOC.

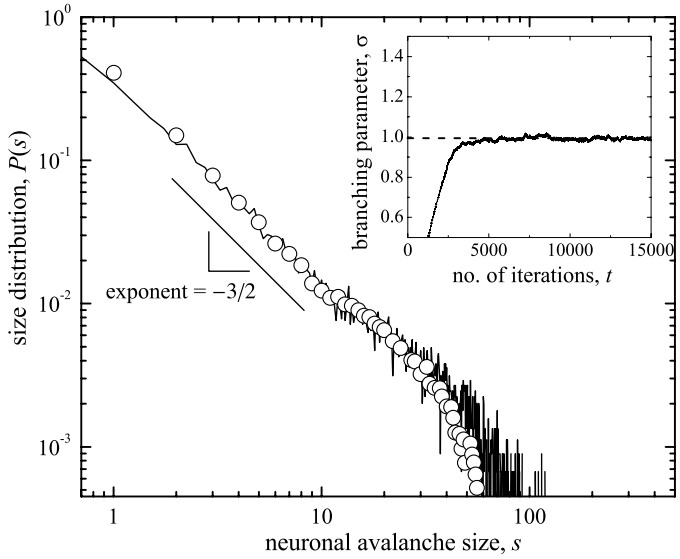

Figure 5. Distribution of neuronal avalanche size (○, data adopted from [3]), and of a simulated network (——) with $\eta N \approx 3\,670$ having a level of non-conservation $\epsilon = 0.25$. The inset graph shows $\sigma(t)$ as a function of time t, approaching the critical value of 1 at the steady-state.

The second limiting case corresponds to $\eta N \gg \theta$, which leads to $\rho^* \to \rho_c$. At this limit, the non-conservative system is always critical. A closer look at figure 4 reveals that the data points lie infinitesimally close to 1 starting at $\eta N \sim 10^4$. This means that if the network is very large, say $N \sim 10^{11}$ which is typical of normal human brain networks, then for a very wide range of background activity $\eta \in (10^{-7}, 1]$, the non-conservative network is always expected to exhibit SOC behaviour in the form of neuronal avalanche activity. Simulation of the model for various levels of non-conservation ϵ likewise yields an avalanche size distribution $P(s)$ of the form plotted in figure 2.

It is also interesting to note that for $\eta N \simeq \theta$, the fixed-point density ρ^* is highly uncertain to small variations in either η or N. This is the regime describing the abrupt rise from 0 to 1 in figure 4.

5.2. Time-scale separation

Separation of time scales presumes that observations on a system are performed over a finite amount of time and have limited temporal resolution. Thus, the processes that occur in the system are separated into fast processes that happen much faster than the resolution of observation, and dynamic processes that happen on the time scale of observation. In the case of neuronal systems, the neuronal avalanche is the fast, but non-conservative, process, whereas the background activity and external simulation are the dynamic processes. Although the time scales for neuronal avalanche and background activity are separated, both processes are nevertheless coupled through their capacity to affect the density ρ of threshold neurons, and ultimately the branching parameter σ, at any given time t of observation.

5.3. Neuronal avalanches

A simulation of the model is performed for a network with size $N = 131\,071$ with background activity $\eta = 0.028$ such that $\eta N \approx 3670$, and level of non-conservation $\epsilon = 0.25$. After

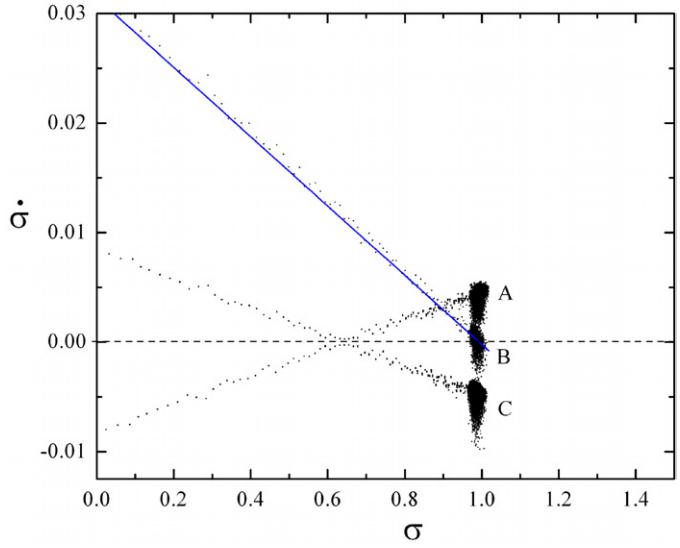

Figure 6. Phase plot of the simulated network converging towards three dynamical attractors: (A) excitatory membrane potential fluctuations; (B) fixed point ($\sigma^* = 1$); (C) inhibitory membrane potential fluctuations. The solid line is the phase portrait based on numerical analysis of (9), neglecting noise $\chi(t)$.

rescaling the simulated avalanche sizes with a factor deduced from experiment [1], the model successfully fits the neuronal avalanche size distribution $P(s)$ adopted from [3], as shown in figure 5. A power-law with exponent $3/2$ primarily characterizes the distribution, as predicted. A cutoff appears because of the limited number of micro-electrodes utilized in resolving LFP intensity during the experiments [1]. The cutoff shifts to the right (i.e., towards larger avalanche sizes) when the number of micro-electrodes is increased. Data from simulation also fit this cutoff remarkably well. The cutoff in the simulation arises from the imposed boundary condition limiting the number of generations of depolarization in a single avalanche. This cutoff also shifts to the right by increasing n. Hence, both model and experimental data agree not only in the power-law behaviour of $P(s)$, but also with regards to the underlying cause of the cutoff. The inset graph illustrates the evolution of the branching parameter σ with time t, approaching the critical value of 1 at the steady state. This steady-state behaviour is supported by a phase plot of σ, shown in figure 6. The fixed point (B) corresponds to $\sigma^* = 1$. Also shown are two other dynamical attractors (A, C), which correspond to the noise $\chi(t)$ that was neglected in the fixed-point analysis of (9). The symmetry between (A) and (C) indicates a balance between cortical excitation and inhibition, which consequently imparts stability to the network's critical steady-state (i.e., σ remains sufficiently close to 1 at any time). Thus, the background activity due to membrane potential fluctuations is essential in letting the network hover around the critical state such that a power-law $P(s)$ is generated.

High redundancy has been regarded as one of the most intriguing characteristics of the human brain. The presence of several identical neurons that perform similar functions may be colligated with robust performance. The robustness of the network's critical behaviour with respect to background intensity is examined by comparing the performance of a small ($N = 131\,071$) and a large ($N = 4194\,303$) network driven by a strong background ($\eta = 1.0$).

Figure 7 (left panel) shows the phase plot of the small network exhibiting imbalance in the excitatory and inhibitory dynamical attractors. There is a notable excursion of the phase plot

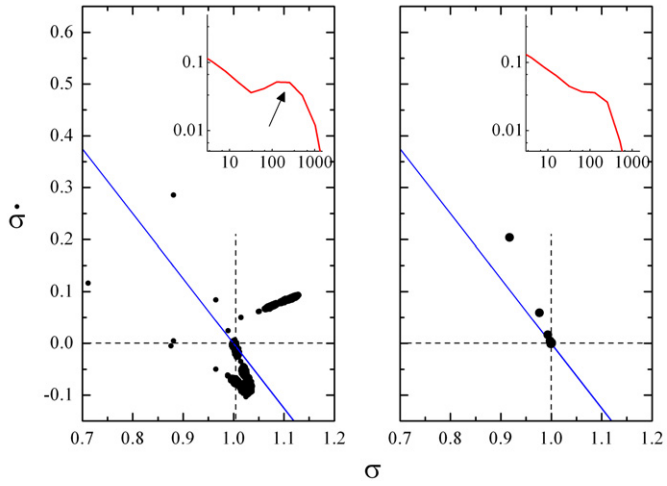

Figure 7. Phase plots for two simulated networks of different sizes N but similar levels of non-conservation $\epsilon = 0.25$ driven by a strong background $\eta = 1.0$. The expected fixed point is at $\sigma^* = 1$. Left panel:— $N = 131\,071$ neurons, showing a prominent excursion at a region where $\sigma > 1$ and $\dot{\sigma} > 0$. The solid line corresponds to mean-field prediction neglecting noise $\chi(t)$. The inset graph displays the resultant logarithmically binned histogram of avalanche sizes, having a marked peak (pointed by arrow) for large sizes, suggestive of *epileptiform activity*. Right panel:— $N = 4194\,303$ neurons, exhibiting fixed-point stability at $\sigma^* = 1$. The inset graph presents the logarithmically binned $P(s)$.

on a region wherein $\sigma > 1$ and $\dot{\sigma} > 0$. This implies that the network is highly excited—i.e., more frequently, a majority of neurons are synchronously firing action potentials. The inset graph reveals a high occurrence probability of large neuronal avalanches as implied by the presence of a hump. High degree of synchronization has been believed to be the precursor of epileptic seizure attacks [17]. Epilepsy is also often attributed to damage of nerve cells resulting from accidents or neuro-degenerative diseases thereby cutting down the network's redundancy, hence its robustness to over-excitation.

On the other hand, figure 7 (right panel) shows that the large network is highly robust even to a strong background intensity. This supports the link between redundancy and robustness. The inset graph of the avalanche size distribution does not exhibit a hump. The large network therefore maintains its critical behaviour despite the intensiveness of membrane potential fluctuations.

6. Summary and conclusion

Recent experimental evidence for SOC discovered in neuronal networks has primarily motivated this research. A non-conservative mean-field sandpile model of SOC has been applied to address the irreconcilability between critical behaviour manifested by the power-law size distribution of neuronal avalanches and the inherent non-conservation of information transmission of neuronal networks in the context of prevailing SOC theory and models. Critical behaviour has been analysed in terms of the theory of branching processes and fixed-point methods. Consequently, it generates scale-invariant avalanche size distributions as demonstrated by theoretical analysis and numerical simulations. The findings provide useful insight into the possible role of membrane potential fluctuations, which effectively generates background activity, on how dissipative neuronal networks maintain a critical state despite

non-conservation. Furthermore, the model has been able to associate network redundancy, which is an intriguing characteristic of brain networks, with network robustness. Small networks which are relatively less redundant than large networks may tip towards epileptiform activity when membrane potential fluctuations are strong.

The NNnM's effectiveness rests on having the branching parameter σ hover around its critical value of 1. A key assumption is that α and β are fixed so that criticality is achieved solely by means of the background activity. Since both α and β act like synaptic efficacy [17], it is possible to generalize the model to the case where α and β fluctuate in time as a result of *synaptic plasticity*—the dynamic adjustment of connection strengths between neurons [4]. Thus, (9) becomes

$$\frac{\mathrm{d}\sigma}{\mathrm{d}t} = \left(2\frac{\partial\alpha}{\partial t} + \frac{\partial\beta}{\partial t}\right)\rho + (2\alpha + \beta)\frac{\partial\rho}{\partial t}.$$

The above generalization is the focus of an upcoming work.

References

[1] Beggs J M and Plenz D 2003 *J. Neurosci.* **23** 11167
[2] Beggs J M and Plenz D 2004 *J. Neurosci.* **24** 5216
[3] Haldeman C and Beggs J M 2005 *Phys. Rev. Lett.* **94** 058101
[4] Vogels T P and Abbott L F 2005 *J. Neurosci.* **25** 10786
[5] Galarreta M and Hestrin S 1998 *Nature Neurosci.* **1** 587
[6] Tsuchiya T and Katori M 2000 *Phys. Rev.* E **61** 1183
[7] Zapperi S, Lauritsen K B and Stanley H E 1995 *Phys. Rev. Lett.* **75** 10786: 4071
[8] Lauritsen K B, Zapperi S and Stanley H E 1996 *Phys. Rev.* E **54** 2483
[9] Carvalho J X and Prado C P C 2000 *Phys. Rev. Lett.* **84** 4006
Drossel B 2002 *Phys. Rev. Lett.* **89** 238701
Boulter C J and Miller G 2003 *Phys. Rev.* E **68** 056108
[10] Socola J E S, Grinstein G and Jayaprakash C 1993 *Phys. Rev.* E **47** 2366
[11] Loreto V, Pietronero L, Vespignani A and Zapperi S 1995 *Phys. Rev. Lett.* **75** 465
[12] Lise S 2002 *J. Phys. A: Math. Gen.* **35** 4641
[13] Hergarten S and Neugebauer H J 2000 *Phys. Rev.* E **61** 2382
Boulter C J and Miller G 2005 *Phys. Rev.* E **71** 016119
[14] Juanico D E, Monterola C and Saloma C 2007 *New J. Phys.* **9** 92
Juanico D E, Monterola C and Saloma C 2007 *Phys. Rev.* E **75** 045105(R)
[15] Monterola C and Saloma C 2002 *Phys. Rev. Lett.* **89** 188102
Monterola C and Zapotocky M 2005 *Phys. Rev.* E **71** 036134
[16] Manna S S 1991 *J. Phys. A: Math. Gen.* **24** L363
[17] Purves D *et al* (eds) 2004 *Neuroscience* 3rd edn (Sunderland, MA: Sinauer Associates)
[18] Simmons P J and Young D (eds) 2003 *Nerve Cells and Animal Behaviour* 2nd edn (Cambridge, MA: Cambridge University Press)
[19] Vespignani A and Zapperi S 1998 *Phys. Rev.* E **57** 6345
[20] Kang S, Kitano K and Fukai T 2004 *Neural Netw.* **17** 307
[21] Mahon S, Cassasus G, Mulle C and Charpier S 2003 *J. Physiol.* **550** 947
[22] Destexhe A and Conteras D 2006 *Science* **314** 85
[23] Meunier C and Segev I 2000 *Handbook of Biological Physics* 4 ed F Moss and S Gielen (Amsterdam: Elsevier) p 426
Kish L B, Harmer G P and Abbott D 2001 *Fluct. Noise Lett.* **1** L13
Longtin A 2002 *Fluct. Noise Lett.* **2** L183
Ginzburg S L and Pustovoit M A 2003 *Fluct. Noise Lett.* **3** L265
Arecchi F T 2005 *Fluct. Noise Lett.* **5** L163
[24] Harris T E 1963 *The Theory of Branching Processes* (Berlin: Springer)
[25] Pinho S T R and Prado C P C 2003 *Braz. J. Phys.* **33** 476
[26] Burroughs S and Tebbens S 2001 *Pure Appl. Geophys.* **158** 741
[27] Strogatz S H 1994 *Nonlinear Dynamics and Chaos: With Applications to Physics, Biology, Chemistry, and Engineering* (Reading, MA: Perseus Books)